JGR Atmospheres

RESEARCH ARTICLE
10.1029/2022JD037709

The Impact of Urbanization on Mesoscale Convective Systems in the Yangtze River Delta Region of China: Insights Gained From Observations and Modeling

Tian Xian[1], Jianping Guo[2], Runze Zhao[1], Tianning Su[3], and Zhanqing Li[3]

[1]State Key Laboratory of Remote Sensing Science, College of Global Change and Earth System Science, Beijing Normal University, Beijing, China, [2]State Key Laboratory of Severe Weather, Chinese Academy of Meteorological Sciences, Beijing, China, [3]Department of Atmospheric & Oceanic Science, ESSIC, University of Maryland, College Park, MD, USA

Key Points:

- Synoptic forcing is a key factor dictating the effect of land cover and land use changes on mesoscale convective systems (MCS)
- Weak (strong) large-scale forcing invigorates (weakens) the vertical development of MCS over and downwind of cities
- The urban heat island effect is more dominant under weak synoptic forcing, whereas the urban-building-barrier effect is more prominent under strong forcing

Correspondence to:
J. Guo and Z. Li,
jpguocams@gmail.com;
zli@atmos.umd.edu

Citation:
Xian, T., Guo, J., Zhao, R., Su, T., & Li, Z. (2023). The impact of urbanization on mesoscale convective systems in the Yangtze River Delta region of China: Insights gained from observations and modeling. *Journal of Geophysical Research: Atmospheres*, *128*, e2022JD037709. https://doi.org/10.1029/2022JD037709

Received 23 AUG 2022
Accepted 9 JAN 2023

Author Contributions:
Conceptualization: Tian Xian, Jianping Guo, Runze Zhao, Tianning Su, Zhanqing Li
Data curation: Tian Xian, Jianping Guo, Runze Zhao, Tianning Su
Formal analysis: Tian Xian, Jianping Guo, Runze Zhao, Tianning Su, Zhanqing Li
Funding acquisition: Jianping Guo, Tianning Su, Zhanqing Li
Investigation: Tian Xian, Jianping Guo, Runze Zhao, Tianning Su, Zhanqing Li
Methodology: Tian Xian, Jianping Guo, Runze Zhao, Tianning Su, Zhanqing Li
Project Administration: Zhanqing Li
Resources: Tianning Su, Zhanqing Li

Abstract Urbanization is an important factor that may influence the formation and development of clouds and precipitation. In this study, we focus on studying the influence of urbanization on mesoscale convective systems (MCS) over the Yangtze River Delta region in China under different synoptic conditions using a combination of radiosonde, meteorological station, and satellite observations. It demonstrates that synoptic forcing can be used to distinguish the effect of land cover and land use on MCS. When the synoptic-scale forcing is weak, the urban heat island (UHI) is the main factor affecting the vertical development of clouds. The UHI decreases atmospheric stability and enhances horizontal convergence, invigorating clouds over and downwind of cities. On the other hand, when strong synoptic-scale forcing is present, buildings in cities cause clouds to bifurcate upwind of cities, moving around them, primarily through their dynamic effects. The heights of cloud tops in central and downwind parts of cities thus drop. Using the Weather Research and Forecasting model simulations of different atmospheric forcings also demonstrate similar patterns around major urban areas. The joint analyses of observations and model simulations provide new insights into the net effects of urbanization on cloud systems.

Plain Language Summary How the mesoscale convective system (MCS) is affected by urban underlying surface remains largely unknown. Here, we characterize the temporal and spatial variation of MCS in the Yangtze River Delta region by using high-resolution cloud top temperature observations from geostationary satellite. To better isolate the effect of synoptic-scale meteorology, the MCS evolution is explicitly investigated with respect to different synoptic-scale forcing. In the case of strong synoptic forcing, the development of MCS tends to be weakened over and downwind of the urban areas due to the urban-buildings-barrier effect. By comparison, under the weak synoptic forcing, urban heat island effect leads to stronger sensible heat flux, which drives the coupling of planetary boundary layer and cloud, and promotes the development of MCS over and downwind of the urban areas. Further analyses based on Weather Research and Forecasting model simulation verify the observational phenomena. The findings obtained here will help advance our understanding of the net effects of urbanization on cloud systems, which provides new insights for the mechanism of urbanization-induced convective initiation.

1. Introduction

Land-cover and land-use (LCLU) changes disrupt surface energy fluxes and alter convective initiation, affecting regional- and even global-scale meteorology (Han et al., 2014; Sarangi et al., 2018). By changing meteorological conditions such as surface temperature, urban areas greatly change the thermodynamic conditions of their surroundings, which, in turn, affects the synoptic process. However, it is unclear how LCLU affects the atmospheric processes of clouds and convection (Theeuwes et al., 2019).

In recent years, climate change, especially regional climate change caused by LCLU, has attracted widespread attention. Dating to the last century, studies have revealed that urbanization can affect the frequency, intensity, and spatial distribution of precipitation (Changnon, 1968; Horton, 1921; Huff & Vogel, 1978). With the development of METROMEX experiments (Changnon et al., 1977) and numerical models (Hjelmfelt, 1982), several studies began exploring the mechanisms by which urban areas affect precipitation. Changnon (1979) found that large cities like St. Louis in the USA have a potential impact on rainfall patterns. Also, the urban heat island (UHI) in Beijing increases the surface temperature, reducing stability within the boundary layer, thereby increasing

Software: Tian Xian, Runze Zhao, Zhanqing Li
Supervision: Jianping Guo, Tianning Su, Zhanqing Li
Validation: Jianping Guo, Tianning Su, Zhanqing Li
Visualization: Tian Xian, Runze Zhao, Zhanqing Li
Writing – original draft: Tian Xian, Runze Zhao
Writing – review & editing: Jianping Guo, Tianning Su, Zhanqing Li

precipitation over and downwind of the city (Shepherd et al., 2002), especially in summer (Y. Zhang et al., 2017). However, Shastri et al. (2015) showed that the UHI had a negligible effect on rainfall compared to the effect of large-scale forcing. In the presence of strong winds or weak UHI, cities mainly affect rainfall through their dynamic effects (Bornstein & Lin, 2000; Bornstein, 2011; Y. Zhang et al., 2017; Dou et al., 2020). Due to the urban-building-barrier effect, storms bifurcate over cities as they pass over them, resulting in reduced rainfall in both urban centers and downwind areas (Atkinson, 1985; Dou et al., 2015, 2020; Niyogi et al., 2017). The feedback mechanism of cities to rainfall is thus still uncertain.

Most previous studies have focused on studying the effects of cities on precipitation. Although clouds are associated with convection and precipitation, only a few studies have examined clouds associated with cities (Theeuwes et al., 2019). Mesoscale convective systems (MCS) is generally defined as thunderstorm clusters, normally exceeding 100 km spatially and 3 hr or more. In addition to producing large amounts of rainfall, MCS is closely associated with such severe weather systems as those associated with hailstone, flood, thunderstorm, and strong wind (Houze, 2004). A recent survey of near-global satellite observations shows that MCSs contribute significantly to urban warm-season precipitation and hydrologic cycle (Feng et al., 2021). MCS is also one of the major convective systems affecting the summertime rainfall episodes across China (D. D. Chen et al., 2019; J. H. Chen et al., 2019, 2020). They seem to have a preferential occurrence in the middle and lower reaches of the Yangtze River Delta (YRD, Cheng et al., 2022). Nevertheless, it remains unclear how the MCS responds to local urban influences in the lower reaches of YRD region. This study, therefore, focuses on MCS rather than rainfall, which is more complex to the urban response. Due to the combined effects of land cover and the climatic context, it is difficult to identify the dominant factor of the urbanization effect. Here, we investigate factors that influence MCS by distinguishing the urban effect on MCS under different synoptic conditions.

2. Data and Methods

2.1. Data

Since the 1980s, the YRD region has experienced the most globally rapid economic development and intensive urbanization at an arguably unparalleled pace. The accelerating urban expansion could lead to a very strong UHI. In the highly populated East Asia, influenced by the very active East Asian monsoon, rapid urbanization may have a notable impact on the weather and climate of the region. East Asia was thus chosen as our study area (Figure 1a). The boundaries of urban areas were delineated using high-quality urban land-use products from 2018 (Gong et al., 2020), developed from high-resolution satellite imagery (as fine as 10 m).

The temporal variation of the urban ratio clearly shows a rapid increase in the YRD region starting around the 1990s (Figure 1c). The urban ratio is the ratio of urban land-use grids to total grids in the YRD region. All land-use grids were obtained from the Resources and Environment Scientific Data Center of the Chinese Academy of Sciences.

High-resolution meteorological observations from 156 stations (colored dots in Figure 1a) and 6 radiosonde sites (green dots in Figure 1a) in the YRD region were used. Radiosondes were generally launched at least twice a day at 08:00 and 20:00 local time (LT). Data were compiled and released by the China Meteorological Administration (http://data.cma.cn/en) and further subject to strict quality control (Guo et al., 2021). The heights of the planetary boundary layer (PBL) and cloud base were obtained from the sounding profiles using the potential temperature gradient method and the WR95 method (Wang & Rossow, 1995), respectively. Note that this study focuses on the warm season (from April to September 2020), when convection is most active (Ding & Chan, 2005).

MCS were identified from the FengYun-2 (FY2) cloud-top temperature (CTT) product (Barton et al., 2021). Synoptic conditions and surface sensible heat fluxes at 1400 LT were analyzed according to European Centre for Medium-Range Weather Forecasts Reanalysis v5 (ERA5) data. Initial and lateral boundary conditions for Weather Research and Forecasting (WRF) model simulations were derived from the National Centers for Environmental Prediction Final (FNL) reanalysis data.

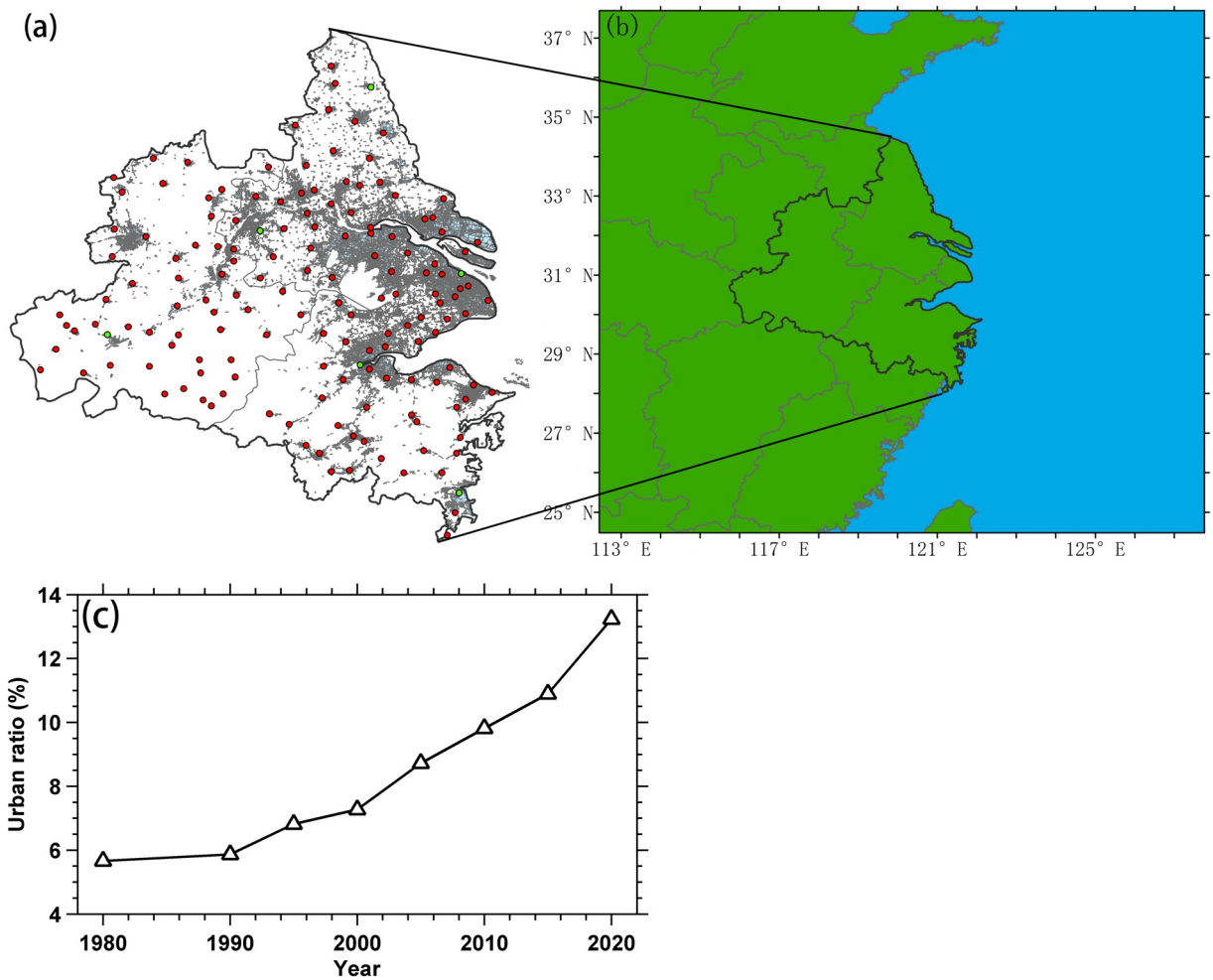

Figure 1. (a) Spatial distribution of urban areas over the lowest reaches of the Yangtze River Delta region (YRD, gray shaded areas) in 2018 from high-quality urban land-use products (Gong et al., 2020) and national-level meteorological stations (colored dots). Green dots represent those weather stations with collocated radiosonde observations. (b) Map of the WRF domain. (c) Time series of urban ratio (%) in this study area shown in (a) during the period 1980 to 2020.

2.2. Classification of Synoptic Patterns

The T-mode obliquely rotated principal component analysis (T-PCA) (Yan et al., 2019) was used to identify dominant synoptic patterns at the 850-hPa geopotential height field at 1400 LT over the YRD region. Compared with other classification methods, the T-PCA is more objective, so has widely been used in studying atmospheric circulation (Huth et al., 2008; Ye et al., 2016). According to previous studies (J. P. Zhang et al., 2012; Ye et al., 2016), the number of reserved principal components was defined as nine, of which six typical synoptic flow patterns were analyzed here.

2.3. Identification and Tracking of MCS

MCS are defined as emerging, rapidly cooling, continuous cloud areas with CTTs less than 235 K and lasting ≥3 hr. Previous work utilized CTTs to identify MCS (Vila et al., 2008; Ai et al., 2016). Arkin and Meisner (1987) and Laurent et al. (2002) employed 235 K as the threshold for identifying MCS. The MCS tracking algorithm used here follows D. D. Chen et al. (2019), J. H. Chen et al. (2019), combining the area-overlapping and Kalman filter (KF) methods. Compared with traditional tracking methods, the algorithm has proven accurate for tracking small and fast-moving MCS (Huang et al., 2018).

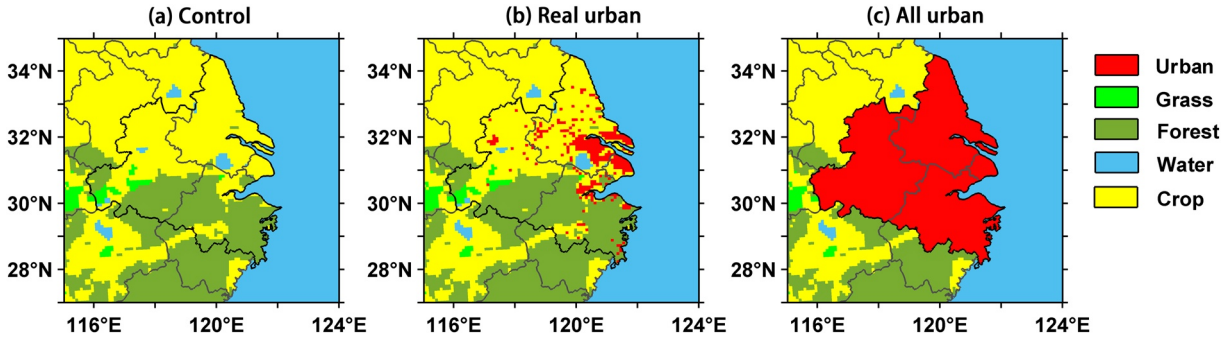

Figure 2. Geographic distribution of land-cover and land-use (LCLU) used for the sensitivity experiments: (a) "Control," (b) "Real urban," and (c) "All urban" in this study area implemented in the WRF model simulations.

There are three main steps to identify MCS from the geostationary satellite FY2: (a) select all pixels with CTT less than 235 K on the satellite image; (b) mark the eligible pixels selected in (a) as 1, and the others as 0; (c) connect zones composed of adjacent pixels as MCS.

An area-overlapping method is then applied to track the identified MCS binary images. Assuming that MCS_m^i is the mth MCS at the ith moment, MCS_n^{i+1} is the nth MCS at the $i+1$th moment. If the overlap ratio of MCS_m^i and MCS_n^{i+1} is greater than or equal to the threshold set in D. D. Chen et al. (2019), J. H. Chen et al. (2019), they are considered to be in the same cloud cluster. However, this method fails for small or fast moving MCS. In this case, the KF method is applied. The motion of MCS_m^i is first predicted by the Kalman equation, followed by finding one closest to the predicted position among all non-overlapping MCS^{i+1} and matching them as the same group of cloud clusters. Huang et al. (2018) describe the basic principles and equations of the KF method.

2.4. Model System Settings

The WRF model (version 4.1.5) was applied to simulate two precipitation processes in Shanghai in the warm season of 2020. Sensitivity experiments examined the impact of urbanization on clouds and precipitation in the YRD region. A single-layer grid with a horizontal resolution of 9 km was used (Figure 1b shows the spatial domain of the study). To simulate real urban land use, based on the US Geological Survey (USGS) LCLU categories, urban land-use data in 2018 (gray shaded areas in Figure 1a) were used to determine the grid points of the urban underlying surface within the model area (Figure 2b). Figure 2 shows the detailed LCLUs of the three experiments conducted to investigate responses to LCLU changes, that is, "Control," "Real urban," and "All urban LCLU." The "Real urban" experiment represents the "present" (2018) urbanization level (Figure 2b). The "All urban" experiment represents super-urbanization, designating the entire YRD region as urban (Figure 2c). In the "Control" experiment, LCLU was set to USGS default conditions LCLU (Figure 2a). Differences between different sets of sensitivity experiments were used to infer the effect of urbanization. The first 24 hr were discarded as model spin-up, and the output of the next 24 hr was retained for analysis. Table 1 summarizes the parameterization schemes used in the WRF model.

Table 1
Parameterization Schemes Used in Model Simulations

Physical processes	Parameterization scheme
Land-surface process	Noah land surface model (F. Chen et al., 1996)
Microphysics	Single-moment 6-class scheme (Hong et al., 2004)
Longwave radiation	RRTM scheme (Mlawer et al., 1997)
Shortwave radiation	Dudhia scheme (1989)
Planetary boundary layer	Yonsei University scheme (Hong et al., 2006)
Cumulus parameterization	Kain-Fritsch scheme (Kain, 2004)

Note. RRTM, rapid radiative transfer model.

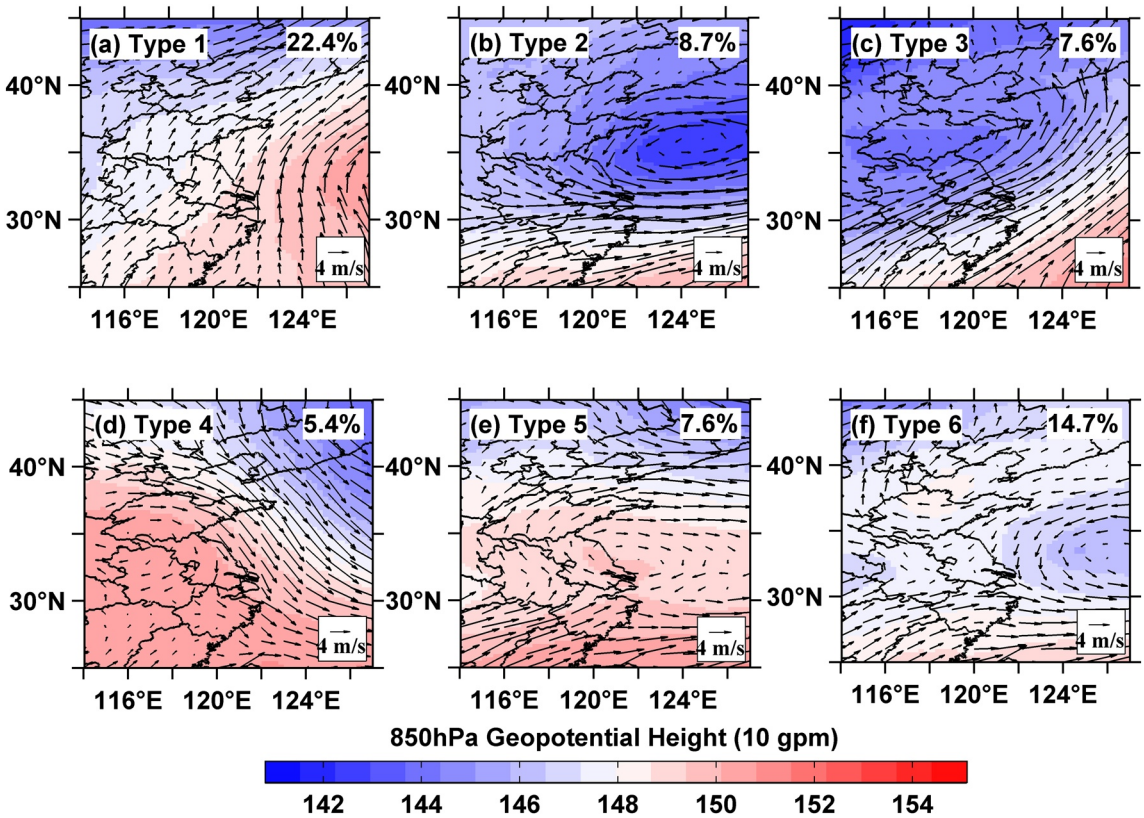

Figure 3. Six dominant synoptic patterns in the YRD region determined by the T-mode obliquely rotated principal component analysis (T-PCA). The color-shading represents 850-hPa geopotential heights (unit: 10 gpm), and black arrows denote the wind vector field (unit: m/s). The percentage in the upper right corner of each panel indicates the frequency of occurrence for each type of synoptic pattern.

3. Results

3.1. Dominant Synoptic Patterns in the YRD

Weather systems can affect the occurrence and development of MCS by affecting the thermodynamic conditions of the atmosphere. T-PCA was thus used to determine the dominant synoptic patterns in the YRD (Figure 3). Based on the ERA5 reanalysis 850-hPa geopotential height field, we divided dominant synoptic patterns in the YRD into strong- and weak-forcing systems. A strong forcing system usually refers to those systems accompanied by extensive precipitation (e.g., frontal and cyclone). The strong-forcing system includes types 1, 2, and 3. Type 1 is controlled by a strong high-pressure system over eastern YRD, similar to the "high pressure in the east and low pressure in the west" pattern (Tao, 1980; Yan et al., 2019). Southerly winds dominate the region, bringing in marine air masses conducive to the occurrence of MCS. Type 2 is ahead of a cold front, where the cold air brought in by northerly winds lifts the warm and moister air masses, generating MCS more easily near the front. Type 3 is controlled by the western Pacific subtropical high with prevailing southwesterly winds, bringing in plentiful water vapor. Overall, these three synoptic patterns are related to large-scale synoptic systems, which are favorable for MCS occurrence. The weak-forcing system includes types 4 (high pressure), 5 (anticyclone), and 6 (uniform pressure field), where the generation of MCS is more likely to be affected by local uplift.

3.2. The Impact of Urbanization on MCS Under Different Synoptic Conditions

Different studies have documented high storm and rainfall anomalies downwind of cities. To assess downwind characteristics for different synoptic types, the 850-hPa wind field at 1400 LT was used to determine the downwind direction, averaged separately for each type to generate streamlines. Figure 4 shows normalized frequencies of MCS in the YRD under the dominance of different synoptic types. Here, a typical cosmopolitan city, Shanghai, is taken as an example. Consistent with previous observations (Bornstein & Lin, 2000; Dou et al., 2015; Niyogi

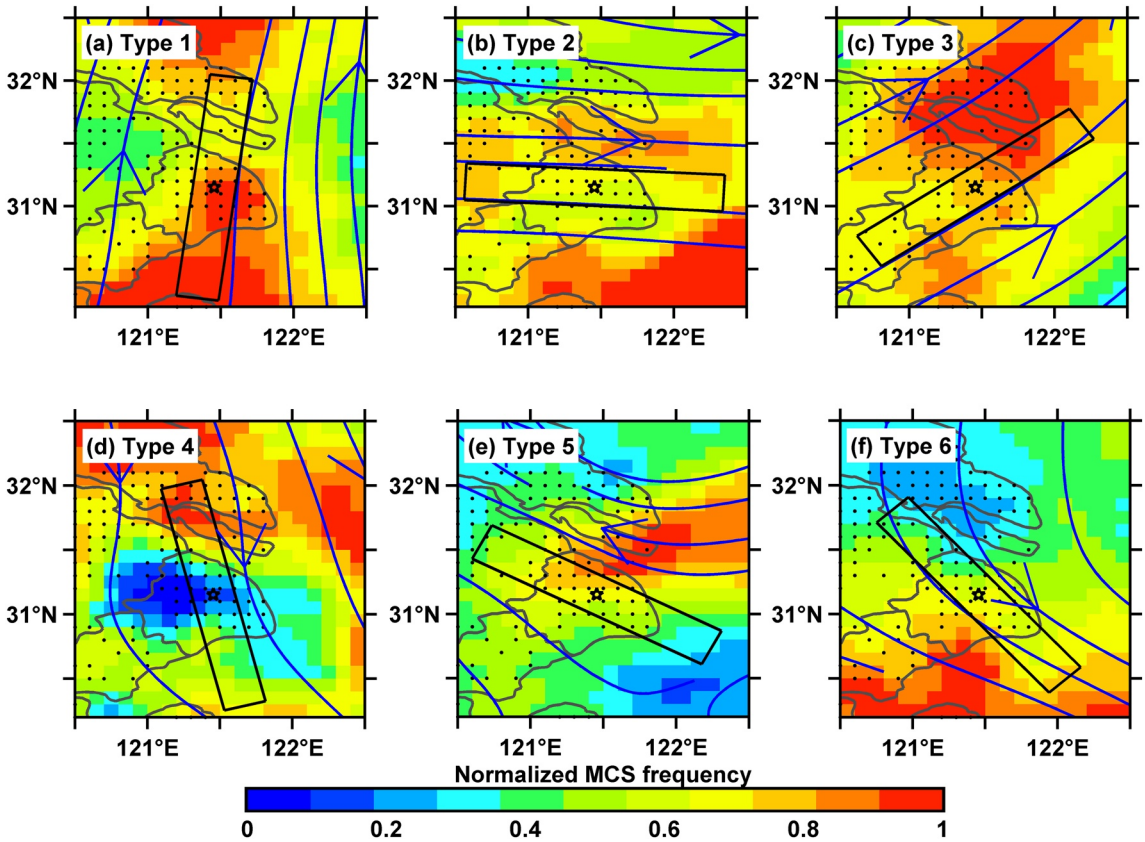

Figure 4. Normalized frequencies of MCS for different dominant synoptic types in the YRD from April to September 2020. Blue arrows are streamlines of the 850-hPa wind field. The star is the geometric center of the Shanghai area, black dots show the urban grid, and black rectangles (200 × 30-km) are downwind cross-sections used to calculate cloud-top temperature gradients.

et al., 2017), summertime MCS appeared most frequently in the urban side edges or downstream areas, that is, lateral boundary convergence zones. Bornstein and LeRoy (1990) call this the building-barrier effect. Different urban cases show similar overall diversion patterns over cities.

The MCSs are often associated with extreme rainfall, and CTT is a useful proxy for rainfall intensity (Klein et al., 2018). Tracking changes in MCS structures can help better predict these extreme events. We analyzed CTTs of downwind cross-sections through the urban center for all synoptic types to better visualize MCS changes in urban areas. For strong-forcing synoptic regimes, a positive downwind CTT gradient was found within the urban area (shaded areas in Figures 5a–5c). For weak synoptic forcing regimes, there is a negative downwind CTT gradient (shaded areas in Figures 5d–5f). This phenomenon illustrates that there may be different urban effects dominating MCS development depending on the scale of the synoptic system in place. Cities have an invigoration effect on the vertical development of clouds in the absence of a large-scale weather system and a weakening effect in the presence of a large-scale weather system. Previous observations by Bornstein and LeRoy (1990) have shown that UHI convergence over urban centers can trigger convection in the absence of large-scale weather systems. With weather systems and wind speeds strengthening, thunderstorms begin to bifurcate, moving into surrounding areas. Subsequent studies have further concluded that when the UHI is weak, the dominant factor in cities is the barrier effect of buildings (Zhang et al., 2017). However, when the UHI is strong, the thermal effect of the UHI is the dominant factor (Zhang et al., 2017). UHI increases the instability of the lower atmosphere by inducing a local circulation, which is beneficial to the formation of convective systems, affecting the distribution of precipitation over urban centers and downwind areas. This explains the opposite downwind CTT gradients under different weather forcing conditions.

Under strong forcing conditions, the weak UHI (0.27°C, Figure 6a) and the high-frequency boundary layer low-level jet [the occurrence probability in the morning (evening) was 35.2% (17.6%)] made the barrier effect

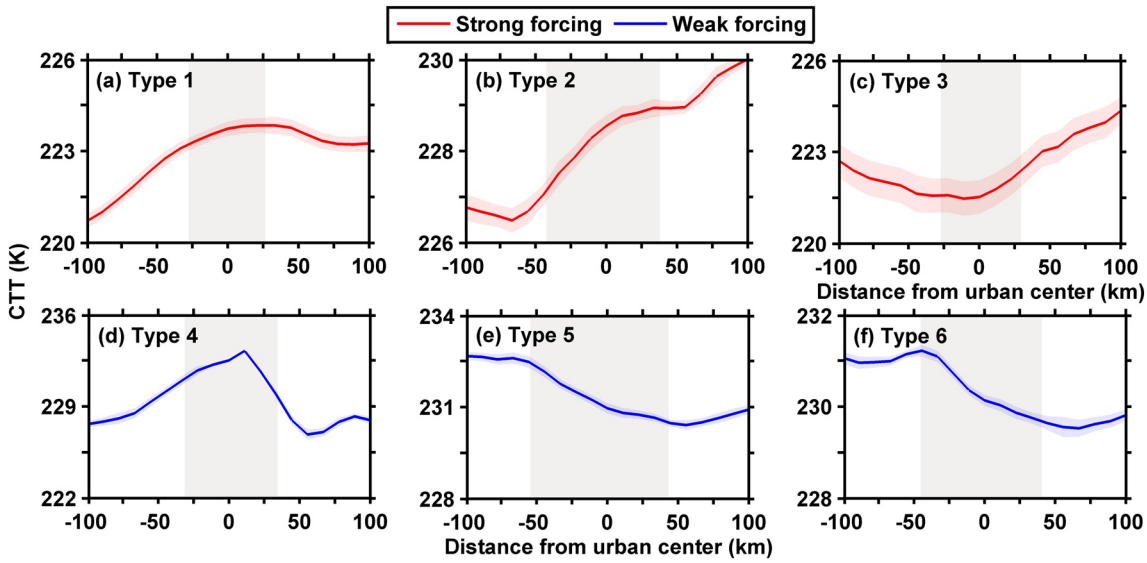

Figure 5. Cross-sections (black rectangles in Figure 4) of the composite mean cloud-top temperature (CTT, unit: K; strong forcing: red solid line, weak forcing: blue solid line) versus distance from the urban center for different synoptic types. Shaded gray areas highlight urban areas, and the red (blue) shading represents one sigma standard deviation of strong forcing (weak forcing).

dominate in the city. The MCS bifurcated and moved around as it passed over the city, weakening clouds in the center and downwind of the city. Under weak forcing conditions, the city had a strong UHI (0.41°C) and a low-frequency, boundary layer low-level jet [22.5% (9.8%) in the morning (evening)] and was dominated by the UHI effect, invigorating clouds over and downwind of the city.

At the same time, according to sounding statistics (Figure 7), strong-forcing weather had a low PBLH and high CBH of 1.46 and 2.85 km, respectively. On the other hand, weak-forcing weather had a higher planetary boundary layer height (PBLH, 1.87 km) and a lower cloud base height (CBH, 2.74 km), favoring the coupling between surface, PBL, and clouds (Su et al., 2022). Under weak synoptic conditions, the relatively strong surface forcing (81.96 W/m^2, Figure 6b) can serve as the driving force for the coupling processes between PBL and clouds. Coupled clouds are sensitive to the changes in the PBL thermodynamics and surface fluxes (Su et al., 2022), thus making them more susceptible to UHIs. Meanwhile, decoupled clouds under strong forcing conditions are less sensitive to UHI disturbances due to their weak linkage with the PBL thermodynamics (the sensible heat forcing is 49.68 W/m^2). Therefore, it is necessary to consider the synoptic background for analyzing the impact of urbanization on clouds. Due to the differences in surface fluxes, PBL, and cloud-surface coupling, we propose that the magnitude of synoptic forcing plays a key role in *n* how urbanization affects convective clouds.

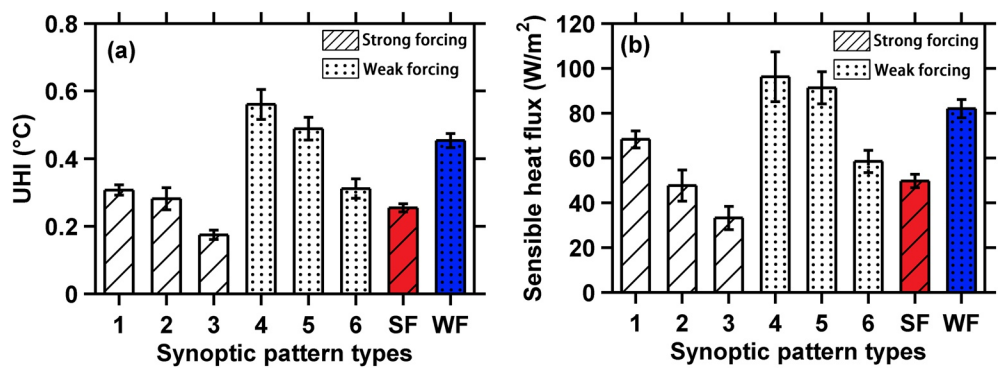

Figure 6. (a) Urban heat island (UHI) intensity (unit: °C), and (b) Surface sensible heat flux (W/m^2) for different synoptic pattern types and weather forcings. SF and WF stand for strong and weak forcings, respectively, and the colored bars for SF (WF) denote the results of the combined average of types 1, 2, 3 (types 4, 5, 6).

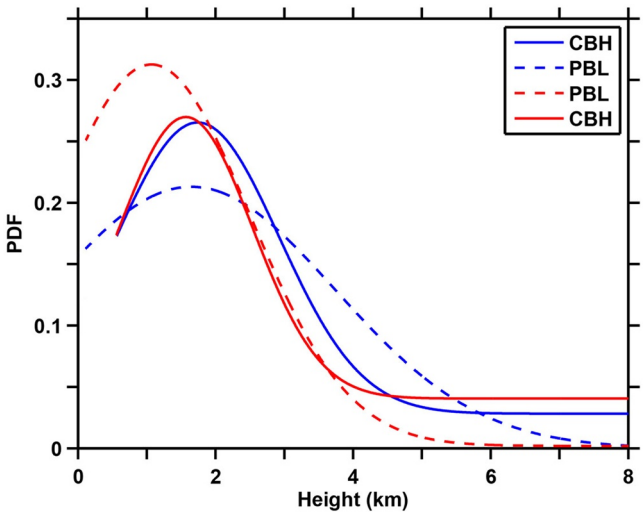

Figure 7. Probability distribution functions (PDFs) of the planetary boundary layer height (PBLH) and cloud-base height (CBH). The blue (red) solid line is the weak-forcing (strong-forcing) CBH, and the blue (red) dotted line is the weak-forcing (strong-forcing) PBLH.

3.3. Simulation of the Impact of Urbanization on MCS

To further understand our observation-based findings, we modeled two cloud systems over the YRD region using the WRF model. These two cases are a typical large-scale weather (pre-cold front) system (29 June 2020) and a local weather (uniform pressure) system (12 September 2020; Figure 8). Simulations were carried out on a domain with a resolution of 9 km and an area of 1,359 × 1,539 km^2. The six-hour FNL reanalysis data set provided initial and lateral boundary conditions for the simulation domain. To capture the effect of cities on clouds, sensitivity experiments were performed only on LCLU changes. By holding all other conditions constant, comparing the three sensitivity experiments reveals the impact of LCLU on the physical forcing of CTT (Sarangi et al., 2018).

Figure 9 compares 24-hr accumulated precipitation amounts from the "Control" experiment and observed at meteorological stations for the two typical cases. The WRF model can model the spatial heterogeneity of accumulated rainfall reasonably well. In the "Real urban" LCLU simulation, the strong-forcing CTT had a positive downwind gradient (Figure 10b), and the weak synoptic forcing CTT had a negative downwind gradient (Figure 11b). The cloud-water mixing ratio of the vertical section in Figure 10 shows that as the urban area expanded, the vertical development of clouds weakened over the city and downwind areas in the strong-forcing process. Figure 12a shows the difference between the simulated maximum reflectivity (Z_{max}) in the "Control" and "Real urban" sensitivity cases. During this period, the convective system moved from the suburbs southwest of the urban area to the central urban area. The movement of the convective system was impeded after the system moved over the urban area in the presence of the city and diverged to the sides of the city. As a result, the convective system strength in the urban area decreased, whereas the strength of the convective system passing through the sides of the urban area increased. For the weak synoptic forcing process, the influence of the city on the vertical development of clouds further increased when the urban area expanded, and the CTT had a larger negative downwind gradient. The vertical wind circulation anomaly in weak forcing indicates that with the expansion of urban LCLU, convergence induces the transfer of enhanced updrafts from the upwind area of Shanghai toward the urban core and downwind directions (Figure 11), enhancing the development of convection. Similar city-land-convective interactions have been reported in previous modeling studies, with significant downstream effects of urban circulation and more rainfall in urban and downwind directions (Schmid & Niyogi, 2017; Shastri et al., 2015; Zhong et al., 2015).

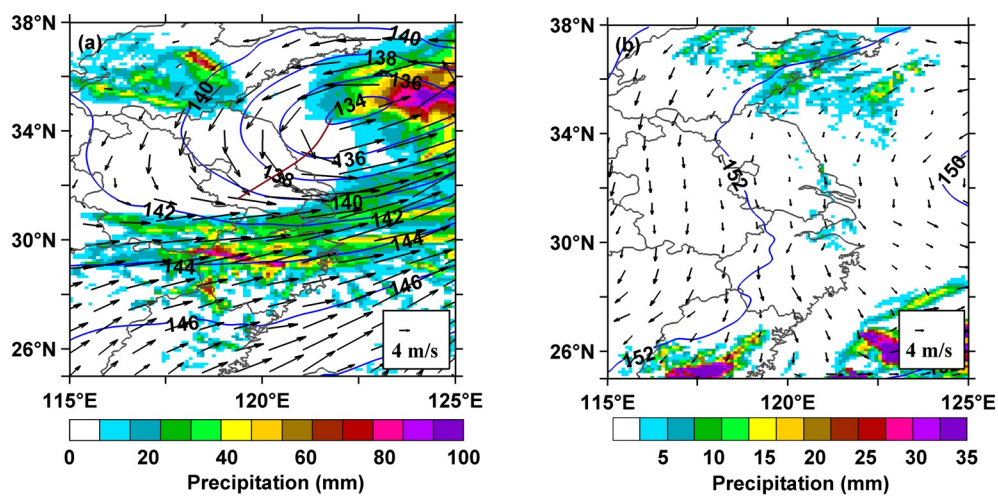

Figure 8. Simulation domains on (a) 29 June 2020 and (b) 12 September 2020. Also shown are the 850-hPa geopotential heights in contours (unit: 10 gpm), 850-hPa wind vectors (arrows, unit: m/s) at 14:00 LT, and 24-hr accumulated precipitation amount (color shaded areas, unit: mm).

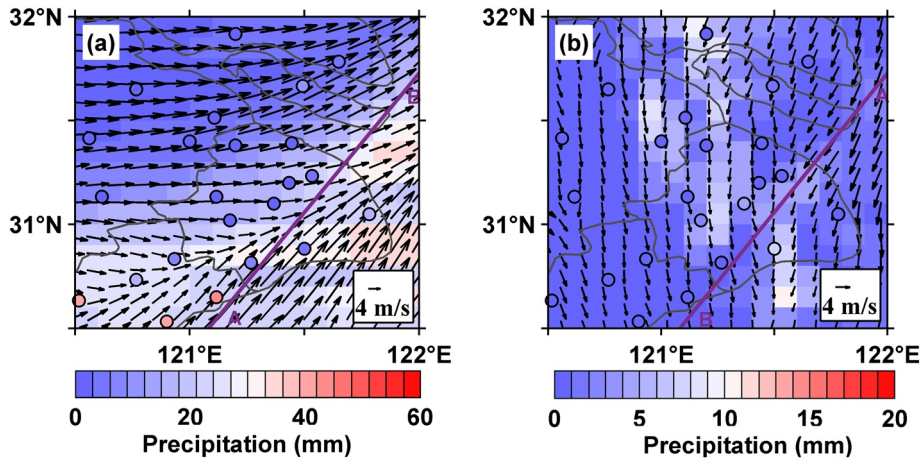

Figure 9. "Control" experiment (colored background) and observed (colored dots) 24-hr accumulated precipitation (unit: mm) and 14:00 LT 850-hPa wind vectors (arrows, unit: m/s) for the model domains on (a) 29 June 2020 and (b) 12 September 2020. The purple solid line (AB) represents the background wind direction.

These simulations suggest that the cooling of the Shanghai urban core and downwind cloud tops is primarily due to associated changes in urban surface properties and updrafts for local weather systems. However, under large-scale weather conditions, urban dynamics rather than thermodynamics dominate. The cloud invigoration mechanism can also explain changes in the city-rainfall association. For local precipitation, stronger updrafts develop as the urban area expands. As a result, the vertical development of clouds may become more active, which in turn will cause rainfall to shift downwind.

4. Conclusions and Discussion

Urbanization is known to have multiple effects on clouds and precipitation, depending on various factors such as meteorological conditions. Although numerical weather prediction can well predict large-scale, persistent convective storms over urban areas, its skill in providing early warnings for locally triggered convective rainfall is relatively poor. To date, urban effects on local convection have not been well addressed by most previous modeling and observational studies.

In this study, we selected urban areas in the YRD in the warm season of 2020 to study the occurrence of MCS and the vertical distribution of associated clouds tracked by geostationary satellites under different weather forcing

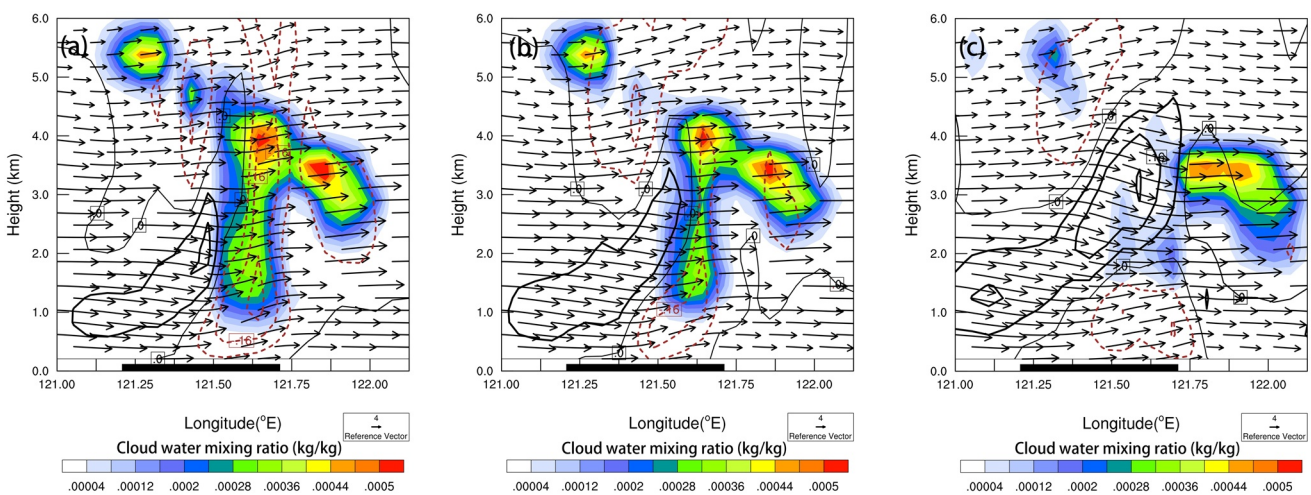

Figure 10. Cloud-water mixing ratio (colored areas, unit: kg/kg) and the vertical distribution of wind vectors (arrows, unit: m/s) along the AB section of (a) the "Control" experiment, (b) the "Real urban" experiment, and (c) the "All urban" experiment at 16:00 LT on 29 June 2020 over Shanghai. The brown dotted (black solid) line represents updrafts (downdrafts).

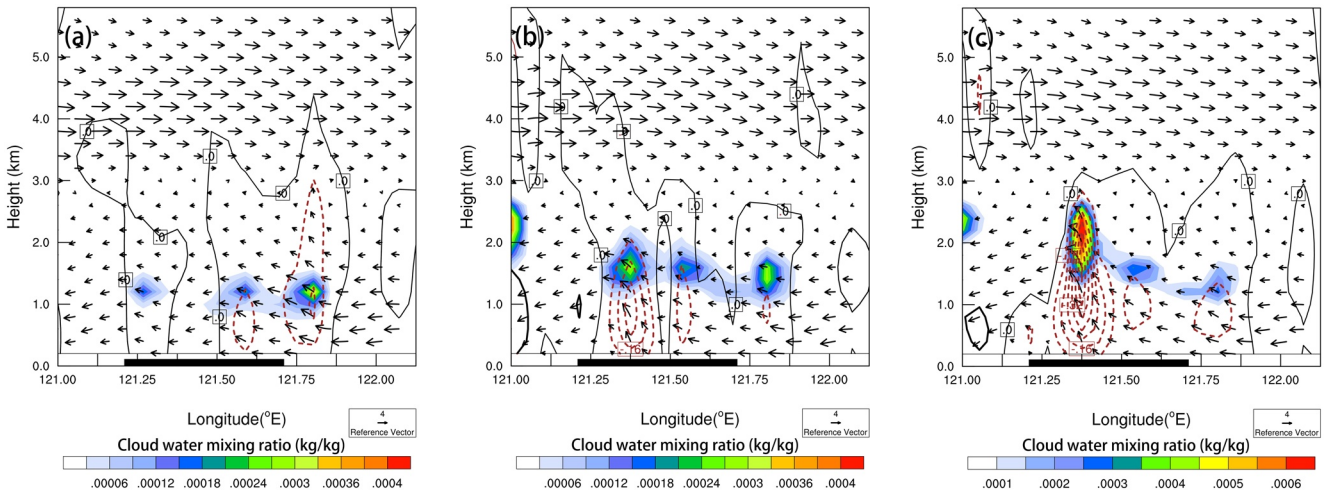

Figure 11. Same as Figure 10, but for 14:00 LT on 12 September 2020.

conditions. The urban effect on MCS in the YRD varies with weather forcing. Weather forcing is an important factor in differentiating the impact of urban LCLU on MCS (Figure 13). Under weak forcing conditions, urban impervious surface results in stronger surface heating rates and higher surface temperature (i.e., UHI effects), which helps form a deeper planetary boundary layer in an urban area. Compared with strong forcing conditions, increases in UHI induce stronger sensible heat flux (Shepherd et al., 2002; Zhu et al., 2016), and the PBL and clouds are more likely to be coupled driven by surface sensible heat forcing. Therefore, increases in surface

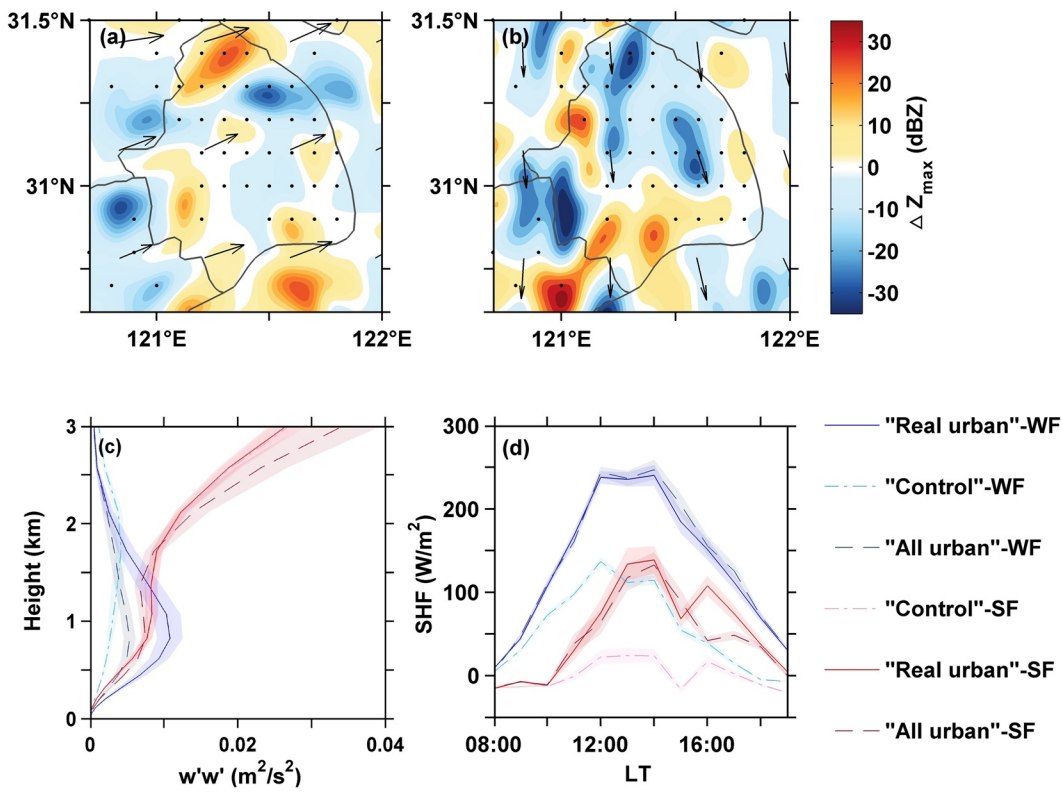

Figure 12. Difference between maximum reflectivity at (a) 15:00 LT on 29 June 2020 and (b) 14:00 LT on 12 September 2020, simulated in the "Real urban" experiment minus that simulated in the "Control" sensitivity experiment (unit: dBZ). Daytime-mean (c) profiles of vertical wind variance and (d) evolution of Surface sensible heat flux (SHF). Strong forcing (Weak forcing) cases are marked in the red (blue) series.

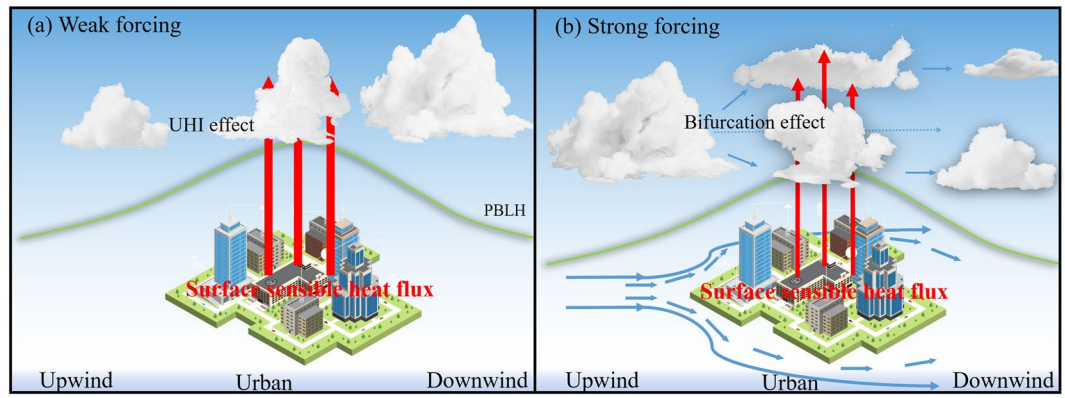

Figure 13. Schematic of urbanization effects on the formation and development of MCS for (a) weak and (b) strong synoptic forcing, respectively.

sensible heat flux in urban areas likely force air parcel above the urban area to quickly lift up. This can cause the low-level atmosphere to form a convergence center, leading to high-reaching convection in central and downwind of cities (Thielen et al., 2000; D. D. Chen et al., 2019; J. H. Chen et al., 2019). For strong forcing, cloud occurrence may become less dependent on surface forcing due to stronger background winds that may induce more stronger wind shear and turbulence (Figure 12c). The atmospheric background wind suppresses the secondary mesoscale circulation due to differential heating of the urban heterogeneous surface through rapid mixing in the PBL and mitigates the impact of urban thermal effects (Lee et al., 2019). Therefore, the building barrier may act as the dominant effect in this case.

Two selected convective cases were well simulated using the 48-hr WRF model with optimal microphysics, cumulus parameterization, and PBL schemes. Convective simulations with weak forcing show that a city will cause updrafts to shift downwind, and sensitivity experiments show that the magnitude of this change will increase as the city expands. In the strong forcing case, as the urban area expands, the high roughness of the urban surface prevents the convective system from moving into the urban area. The convective system cannot easily move over the central urban area, instead bifurcating and moving around the urban area, weakening the vertical development of urban clouds.

This study presents strong evidence that MCS characteristics in the YRD region may result from the interaction between the cloud invigoration effect caused by the UHI and the barrier effect of urban buildings. Note, however, that we are primarily concerned with qualitative results for different weather forcing scenarios, hoping to differentiate the impact of urban effects to some extent through this approach. This study also suggests that more observations, especially vertical profiles of wind, temperature, and humidity in the boundary layer, are needed to elucidate the physical mechanisms of different urban effects on clouds so that further quantitative understanding can be gained.

Data Availability Statement

The radiosonde (Guo, 2022), synoptic surface meteorological data (CMA, 2019), reanalysis data (ECMWF, 2019; NCEP, 2019) and cloud top temperature data from geostationary data (NSMC, 2022) were used in the creation of this manuscript.

Acknowledgments
This research was funded by the National Natural Science Foundation (42030606 and U2142209).

References

Ai, Y., Li, W., Meng, Z., & Li, J. (2016). Life cycle characteristics of MCSs in Middle East China tracked by geostationary satellite and precipitation estimates. *Monthly Weather Review*, *144*(6), 2517–2530. https://doi.org/10.1175/MWR-D-15-0197.1

Arkin, P. A., & Meisner, B. N. (1987). The relationship between large-scale convective rainfall and cold cloud over the western-hemisphere during 1982–84. *Monthly Weather Review*, *115*(1), 51–74. https://doi.org/10.1175/1520-0493(1987)115<0051:TRBLSC>2.0.CO;2

Atkinson, B. W. (1985). *The urban atmosphere*. Cambridge University Press.

Barton, E. J., Taylor, C. M., Klein, C., Harris, P. P., & Meng, X. (2021). Observed soil moisture impact on strong convection over mountainous Tibetan Plateau. *Journal of Hydrometeorology*, *22*(3), 561–572. https://doi.org/10.1175/jhm-d-20-0129.1

Bornstein, R., & Lin, Q. L. (2000). Urban heat islands and summertime convective thunderstorms in Atlanta: Three case studies. *Atmospheric Environment*, *34*(3), 507–516. https://doi.org/10.1016/S1352-2310(99)00374-X

Bornstein, R. D. (2011). Establishment of meso-met modeling case studies to evaluate the relative roles of urban dynamics and aerosols on summer thunderstorms. In *Eighteenth conference on planned and inadvertent weather modification*. American Meteorological Society.

Bornstein, R. D., & LeRoy, G. M. (1990). Urban barrier effects on convective and frontal thunderstorms. In *Fourth conference on mesoscale processes*. American Meteorological Society.

Changnon, S. A. (1968). The La Porte weather anomaly - Fact or fiction? *Bulletin of the American Meteorological Society*, *49*(1), 4–11. https://doi.org/10.1175/1520-0477-49.1.4

Changnon, S. A. (1979). Rainfall changes in summer caused by St. Louis. *Science*, *205*(4404), 402–404. https://doi.org/10.1126/science.205.4404.402

Changnon, S. A., Huff, F. A., Schickedanz, P. T., & Vogel, J. L. (1977). *Summary of METROMEX, volume 1: Weather anomalies and impacts*. Illinois State Water Surv.

Chen, D., Guo, J., Yao, D., Feng, Z., & Lin, Y. (2020). Elucidating the life cycle of warm-season mesoscale convective systems in eastern China from the Himawari-8 geostationary satellite. *Remote Sensing*, *12*(14), 2307. https://doi.org/10.3390/rs12142307

Chen, D. D., Guo, J. P., Yao, D., Lin, Y. L., Zhao, C. F., Min, M., et al. (2019). Mesoscale convective systems in the Asian monsoon region from advanced Himawari imager: Algorithms and preliminary results. *Journal of Geophysical Research: Atmospheres*, *124*(4), 2210–2234. https://doi.org/10.1029/2018JD029707

Chen, F., Mitchell, K., Schaake, J., Xue, Y. K., Pan, H. L., Koren, V., et al. (1996). Modeling of land surface evaporation by four schemes and comparison with FIFE observations. *Journal of Geophysical Research*, *101*(D3), 7251–7268. https://doi.org/10.1029/95jd02165

Chen, J. H., Wu, X. Q., Yin, Y., Lu, C. S., Xiao, H., Huang, Q., & Deng, L. P. (2019). Thermal effects of the surface heat flux on cloud systems over the Tibetan Plateau in boreal summer. *Journal of Climate*, *32*(15), 4699–4714. https://doi.org/10.1175/JCLI-D-18-0604.1

Cheng, T. F., Dong, Q. Z., Dai, L., & Lu, M. Q. (2022). A dual regime of mesoscale convective systems in the East Asian Monsoon annual cycle. *Journal of Geophysical Research: Atmospheres*, *127*(13), 1–21. https://doi.org/10.1029/2022JD036523

CMA. (2019). Meteorological data. China meteorological administration. Retrieved from http://data.cma.cn/

Ding, Y. H., & Chan, J. C. L. (2005). The East Asian summer monsoon: An overview. *Meteorology and Atmospheric Physics*, *89*(1–4), 117–142. https://doi.org/10.1007/s00703-005-0125-z

Dou, J., Bornstein, R., Miao, S., Sun, J., & Zhang, Y. (2020). Observation and simulation of a bifurcating thunderstorm over Beijing. *Journal of Applied Meteorology and Climatology*, *59*(12), 2129–2148. https://doi.org/10.1175/jamc-d-20-0056.1

Dou, J., Wang, Y., Bornstein, R., & Miao, S. (2015). Observed spatial characteristics of Beijing urban climate impacts on summer thunderstorms. *Journal of Applied Meteorology and Climatology*, *54*(1), 94–105. https://doi.org/10.1175/jamc-d-13-0355.1

ECMWF. (2019). ERA5-land reanalysis [Dataset]. MediumRange. Retrieved from https://cds.climate.copernicus.eu/cdsapp#!/dataset/reanalysis-era5-land?tab=overview

Feng, Z., Leung, L. R., Liu, N., Wang, J., Houze, R. A., Jr., Li, J., et al. (2021). A global high-resolution mesoscale convective system database using satellite-derived cloud tops, surface precipitation, and tracking. *Journal of Geophysical Research: Atmospheres*, *126*(8), e2020JD034202. https://doi.org/10.1029/2020jd034202

Gong, P., Chen, B., Li, X. C., Liu, H., Wang, J., Bai, Y. Q., et al. (2020). Mapping essential urban land use categories in China (EULUC-China): Preliminary results for 2018. *Science Bulletin*, *65*(3), 182–187. https://doi.org/10.1016/j.scib.2019.12.007

Guo, J. (2022). Radiosonde profiles released at 0500 UTC over China [Dataset]. Chinese Academy of Meteorological Sciences. https://doi.org/10.5281/zenodo.6415075

Guo, J., Zhang, J., Yang, K., Liao, H., Zhang, S. D., Huang, K. M., et al. (2021). Investigation of near-global daytime boundary layer height using high-resolution radiosondes: First results and comparison with ERA-5, MERRA-2, JRA-55, and NCEP-2 reanalyses. *Atmospheric Chemistry and Physics*, *21*(22), 17079–17097. https://doi.org/10.5194/acp-21-17079-2021

Han, J. Y., Baik, J. J., & Lee, H. (2014). Urban impacts on precipitation. *Asia-Pacific Journal of Atmospheric Sciences*, *50*(1), 17–30. https://doi.org/10.1007/s13143-014-0016-7

Hjelmfelt, M. R. (1982). Numerical simulation of the effects of St. Louis on mesoscale boundary-layer air-flow and vertical air motion - Simulations of urban vs non-urban effects. *Journal of Applied Meteorology*, *21*(9), 1239–1257. https://doi.org/10.1175/1520-0450(1982)021<1239:NSOTEO>2.0.CO;2

Hong, S. Y., Dudhia, J., & Chen, S. H. (2004). A revised approach to ice microphysical processes for the bulk parameterization of clouds and precipitation. *Monthly Weather Review*, *132*(1), 103–120. https://doi.org/10.1175/1520-0493(2004)132<0103:Aratim>2.0.Co;2

Hong, S. Y., Noh, Y., & Dudhia, J. (2006). A new vertical diffusion package with an explicit treatment of entrainment processes. *Monthly Weather Review*, *134*(9), 2318–2341. https://doi.org/10.1175/mwr3199.1

Horton, R. E. (1921). Thunderstorm breeding spots. *Monthly Weather Review*, *49*(4), 193–194. https://doi.org/10.1175/1520-0493(1921)49<193a:ts>2.0.co;2

Houze, R. A., Jr. (2004). Mesoscale convective systems. *Reviews of Geophysics*, *42*(4), RG4003. https://doi.org/10.1029/2004rg000150

Huang, X., Hu, C., Huang, X., Chu, Y., Tseng, Y. H., Zhang, G. J., & Lin, Y. (2018). A long-term tropical mesoscale convective systems dataset based on a novel objective automatic tracking algorithm. *Climate Dynamics*, *51*(7–8), 3145–3159. https://doi.org/10.1175/1520-0493(1921)49<193a:TS>2.0.CO;2

Huff, F. A., & Vogel, J. L. (1978). Urban, topographic and diurnal effects on rainfall in the St. Louis region. *Journal of Applied Meteorology*, *17*(5), 565–577. https://doi.org/10.1007/s00382-018-4071-0

Huth, R., Beck, C., Philipp, A., Demuzere, M., Ustrnul, Z., Cahynova, M., et al. (2008). Classifications of atmospheric circulation patterns. *Annals of the New York Academy of Sciences*, *1146*(1), 105–152. https://doi.org/10.1196/annals.1446.019

Kain, J. S. (2004). The Kain-Fritsch convective parameterization: An update. *Journal of Applied Meteorology*, *43*(1), 170–181. https://doi.org/10.1175/1520-0450(2004)043<0170:Tkcpau>2.0.Co;2

Klein, C., Belusic, D., & Taylor, C. M. (2018). Wavelet scale analysis of mesoscale convective systems for detecting deep convection from infrared imagery. *Journal of Geophysical Research: Atmospheres*, *123*(6), 3035–3050. https://doi.org/10.1002/2017JD027432

Laurent, H., Machado, L. A. T., Morales, C. A., & Durieux, L. (2002). Characteristics of the Amazonian mesoscale convective systems observed from satellite and radar during the WETAMC/LBA experiment. *Journal of Geophysical Research*, *107*(D20), 8054. https://doi.org/10.1029/2001jd000337

Lee, J. M., Zhang, Y. Y., & Klein, S. A. (2019). The effect of land surface heterogeneity and background wind on shallow cumulus clouds and the transition to deeper convection. *Journal of the Atmospheric Sciences*, *76*(2), 4001–4419. https://doi.org/10.1175/JAS-D-18-0196.1

Mlawer, E. J., Taubman, S. J., Brown, P. D., Iacono, M. J., & Clough, S. A. (1997). Radiative transfer for inhomogeneous atmospheres: RRTM, a validated correlated-k model for the longwave. *Journal of Geophysical Research*, *102*(D14), 16663–16682. https://doi.org/10.1029/97jd00237

NCEP. (2019). Final (FNL) reanalysis data [Dataset]. National Centers for Environmental Prediction (NCEP). Retrieved from https://rda.ucar.edu/

Niyogi, D., Lei, M., Kishtawal, C., Schmid, P., & Shepherd, M. (2017). Urbanization impacts on the summer heavy rainfall climatology over the eastern United States. *Earth Interactions*, *21*(5), 1–7. https://doi.org/10.1175/ei-d-15-0045.1

NSMC. (2022). Cloud top temperature (CTT) [Dataset]. National Satellite Meteorological Centre (NSMC). Retrieved from http://www.nsmc.org.cn/nsmc/cn/home/index.html

Sarangi, C., Tripathi, S. N., Qian, Y., Kumar, S., & Leung, L. R. (2018). Aerosol and urban land use effect on rainfall around cities in Indo-Gangetic Basin from observations and cloud resolving model simulations. *Journal of Geophysical Research: Atmospheres*, *123*(7), 3645–3667. https://doi.org/10.1002/2017jd028004

Schmid, P. E., & Niyogi, D. (2017). Modeling urban precipitation modification by spatially heterogeneous aerosols. *Journal of Applied Meteorology and Climatology*, *56*(8), 2141–2153. https://doi.org/10.1175/jamc-d-16-0320.1

Shastri, H., Paul, S., Ghosh, S., & Karmakar, S. (2015). Impacts of urbanization on Indian summer monsoon rainfall extremes. *Journal of Geophysical Research: Atmospheres*, *120*(2), 496–516. https://doi.org/10.1002/2014JD022061

Shepherd, J. M., Harold, P., & Negri, A. J. (2002). Rainfall modification by major urban areas: Observations from spaceborne rain radar on the TRMM satellite. *Journal of Applied Meteorology*, *41*(7), 689–701. https://doi.org/10.1175/1520-0450(2002)041<0689:RMBMUA>2.0.CO;2

Su, T. N., Zheng, Y. T., & Li, Z. Q. (2022). Methodology to determine the coupling of continental clouds with surface and boundary layer height under cloudy conditions from lidar and meteorological data. *Atmospheric Chemistry and Physics*, *22*(2), 1453–1466. https://doi.org/10.5194/acp-22-1453-2022

Tao, S. (1980). *Torrential rains in China* (pp. 115–121). Science Press.

Theeuwes, N. E., Barlow, J. F., Teuling, A. J., Grimmond, C. S. B., & Kotthaus, S. (2019). Persistent cloud cover over mega-cities linked to surface heat release. *NPJ Climate and Atmospheric Science*, *2*(1), 15. https://doi.org/10.1038/s41612-019-0072-x

Thielen, J., Wobrock, W., Gadian, A., Mestayer, P. G., & Creutin, J. D. (2000). The possible influence of urban surfaces on rainfall development: A sensitivity study in 2D in the meso-gamma-scale. *Atmospheric Research*, *54*(1), 15–39. https://doi.org/10.1016/S0169-8095(00)00041-7

Vila, D. A., Machado, L. A. T., Laurent, H., & Velasco, I. (2008). Forecast and Tracking the Evolution of Cloud Clusters (ForTraCC) using satellite infrared imagery: Methodology and validation. *Weather and Forecasting*, *23*(2), 233–245. https://doi.org/10.1175/2007waf2006121.1

Wang, J. H., & Rossow, W. B. (1995). Determination of cloud vertical structure from upper-air observations. *Journal of Applied Meteorology and Climatology*, *34*(10), 2243–2258. https://doi.org/10.1175/15200450(1995)034<2243:DOCVSF>2.0.CO;2

Yan, Y., Miao, Y. C., Guo, J. P., Liu, S. H., Liu, H., Lou, M. Y., et al. (2019). Synoptic patterns and sounding-derived parameters associated with summertime heavy rainfall in Beijing. *International Journal of Climatology*, *39*(3), 1476–1489. https://doi.org/10.1002/joc.5895

Ye, X. X., Song, Y., Cai, X. H., & Zhang, H. S. (2016). Study on the synoptic flow patterns and boundary layer process of the severe haze events over the North China Plain in January 2013. *Atmospheric Environment*, *124*, 129–145. https://doi.org/10.1016/j.atmosenv.2015.06.011

Zhang, J. P., Zhu, T., Zhang, Q. H., Li, C. C., Shu, H. L., Ying, Y., et al. (2012). The impact of circulation patterns on regional transport pathways and air quality over Beijing and its surroundings. *Atmospheric Chemistry and Physics*, *12*(11), 5031–5053. https://doi.org/10.5194/acp-12-5031-2012

Zhang, Y., Miao, S., Dai, Y., & Bornstein, R. (2017). Numerical simulation of urban land surface effects on summer convective rainfall under different UHI intensity in Beijing. *Journal of Geophysical Research: Atmospheres*, *122*(15), 7851–7868. https://doi.org/10.1002/2017jd026614

Zhong, S., Qian, Y., Zhao, C., Leung, R., & Yang, X. Q. (2015). A case study of urbanization impact on summer precipitation in the greater Beijing metropolitan area: Urban heat island versus aerosol effects. *Journal of Geophysical Research: Atmospheres*, *120*(20), 10903–10914. https://doi.org/10.1002/2015jd023753

Zhu, X. L., Ni, G. H., Cong, Z. T., Sun, T., & Li, D. (2016). Impacts of surface heterogeneity on dry planetary boundary layers in an urban-rural setting. *Journal of Geophysical Research: Atmospheres*, *121*(20), 12164–12179. https://doi.org/10.1002/2016JD024982